Giant, low-loss magnetic responses and ultraslow magnetic solitons via plasmon-induced transparency

Yibin Xu,[1] Zhengyang Bai,[1] and Guoxiang Huang[1,2,3]

[1]*State Key Laboratory of Precision Spectroscopy, East China Normal University, Shanghai 200062, China*
[2]*NYU-ECNU Joint Institute of Physics, New York University Shanghai, Shanghai 200062, China*
[3]*Collaborative Innovation Center of Extreme Optics, Shanxi University, Taiyuan, Shanxi 030006, China*

(Received 14 February 2020; accepted 12 May 2020; published 29 May 2020)

The realization of advanced materials with strong, low-loss, and pure magnetic responses to radiation fields both in linear and nonlinear regimes is an important and long-standing goal for fundamental physics and practical applications. Here, we propose a physical scheme for obtaining such responses by using a metamaterial constructed by an array of unit cells consisting of two coupled varactor-loaded split-ring resonators working under the condition of plasmon-induced transparency (PIT). We show that the PIT in such metamaterial not only significantly suppresses radiation absorption but also greatly enhances magnetic Kerr nonlinearity, which may be many orders of magnitude larger than that obtained by conventional magnetic materials reported up to now. Based on such a nonlinear metamaterial, we further show that stable magnetic solitons with ultraslow propagation velocity and very low generation power can be created. Our research opens a route for designing novel metamaterial devices with strong, low-loss, pure, and actively tunable magnetic responses and for obtaining stable and low-power nonlinear magnetic pulses, which are promising for applications in information processing and transmission.

DOI: 10.1103/PhysRevA.101.053859

I. INTRODUCTION

In recent years, much attention has been paid to research on metamaterials, which are artificial electromagnetic media structured on subwavelength scales. Metamaterial research has now become a paradigm for designing a new generation of metadevices that may control the propagation properties of electromagnetic waves with many desired, exotic properties and unprecedented functionalities [1–6].

It is well known that conventional atoms and molecules are rather restrictive for building effective magnetic materials, which is particularly true at or above gigahertz frequencies. The major reason for this is that the magnetic component of electromagnetic radiation in this frequency region couples to atoms or molecules much more weakly than the electric component [3,7]. Thus it is a big challenge to acquire large magnetic responses in microwave frequencies and higher. In a pioneering work, Pendry *et al.* [8] suggested that a large magnetic response may be achieved by using a metamaterial consisting of an array of artificially fabricated photonic atoms (meta-atoms), e.g., split ring resonators (SRRs).

It is a dream for scientists and engineers to obtain nonlinear materials that can outperform naturally available ones. Pendry *et al.* [8] suggested that a metamaterial with enhanced nonlinearity could be realized by doping nonlinear elements at positions of meta-atoms where the radiation field is strong. Based on such an idea, many authors have presented different schemes to enhance metamaterial nonlinearity by the insertion of nonlinear elements, or by the use of nonlinear host materials, etc. Related nonlinear phenomena, including nonlinear self-action, frequency conversion and parametric amplification, surface effects, nonlinear guided waves, and solitons, have been explored. For details, see Refs. [6,9], the review articles [10–12], as well as references cited therein.

Among various efforts, great interest has particularly focused on the investigation of nonlinear metamaterial constructed by an array of magnetic meta-atoms, i.e., varactor-loaded split-ring resonators (VLSRRs) in which each meta-atom consists of a SRR with packaged varactors embedded in its capacitive gaps [13–21]. The main reason to do this is that the meta-atoms in such metamaterial have a dominant magnetic response, and the magnetic nonlinearity contributed by the varactors can be manipulated actively. However, all reported works on the linear and nonlinear magnetic responses based on such metamaterials are confronted with some serious problems, including large radiation loss and high input power for radiation propagation over a long distance, etc.

In this work, we propose a scheme to realize strong, low-loss, and pure magnetic responses in both linear and nonlinear regimes by using a metamaterial constructed by an array of magnetic meta-atoms consisting of two coupled VLSRRs working under the condition of plasmon-induced transparency (PIT). PIT [22–31] is an interesting classical analog of electromagnetically induced transparency (EIT) occurring typically in there-level atomic systems [32–36]. We demonstrate that the PIT in such metamaterials not only significantly suppress radiation absorption but also greatly enhance the magnetic Kerr nonlinearity of the system, which can be more than ten orders of magnitude greater than those obtained by conventional magnetic materials [6,9]. As a result, the problems of large radiation loss and high input power for radiation propagation in metamaterials can be satisfactorily avoided.

Based on the giant magnetic Kerr nonlinearity obtained in such metamaterials, we further demonstrate that nonlinear magnetic pulses, i.e., magnetic solitons, with ultraslow propagation velocity and very low generation power, can be created and propagate stably in the system. Our research has major significance because the results obtained can be used for designing novel metamaterial devices with strongly nonlinear, low-loss, pure, and actively tunable magnetic responses, and for generating stable and low-power nonlinear magnetic pulses, which are not only interesting for the exploration of fundamental physics of metamaterials but also promising for applications in information processing and transmission.

The remainder of the article is arranged as follows: In Sec. II, we describe the physical model. In Sec. III, we present the numerical and analytical results on linear magnetic excitations, derive the nonlinear envelope equation for nonlinear magnetic pulses, and discuss the giant magnetic Kerr nonlinearity of the system. In Sec. IV, we study the ultraslow and low-power magnetic solitons and discuss their stability. The last section (i.e., Sec. V) gives a summary of the main results obtained in this work.

II. MODEL

The metamaterial structure proposed here is a periodic array of unit cells (magnetic meta-atoms) consisting of two SRRs (i.e., SRR1 and SRR2) with (nonlinear) varactors inserted into their slits (capacitive gaps) [see Fig. 1(a)]. The geometry of each SRR is assumed to be $l \times l = 8 \times 8$ mm^2; aluminum strips with thickness $w = 0.5$ mm that form the SRR-pair pattern can be etched, for example, on a Si-on-sapphire wafer comprised of a 1-mm-thick undoped Si film and a 2.1-mm-thick sapphire substrate. To realize a nonlinear magnetic response, a varactor is assumed to be inserted in each capacitive gap of the SRR1 and SRR2 with size $h = 0.2$ mm. A schematic of the metamaterial structure is illustrated in Fig. 1(c).

For convenience, we assume the incident (microwave) radiation field is along z direction, with the electric field **E** (magnetic field **H**) along x (y) direction. For obtaining a dominant magnetic response, **H** is chosen to be parallel to the normal direction of the SRR1 (functioning as a magnetic dipole), i.e., along the y direction [see Fig. 1(a)]. In this situation, the incident radiation field couples with SRR1 directly and stimulates a localized surface-plasmon resonance, and hence the SRR1 manifests as a bright magnetic oscillator to the radiation field [15]. However, because of the normal direction perpendicular to **H**, SRR2 does not manifest as a bright magnetic oscillator but instead as a dark magnetic oscillator; it can only have an indirect weak coupling to the radiation field through the coupling with SRR1 [24].

According to the need for a practical design, one can vary the spatial dimensions of the SRR1 and SRR2 to tune their resonance frequencies. Here we assume that the resonance frequency of the dark oscillator SRR2 coincides nearly with that of the bright oscillator SRR1. When the varactors are inserted in capacitive gaps of the SRR1 and SRR2, each meta-atom (i.e., the VLSRR) can still be well modeled as an RLC circuit model with external excitation, as sketched in Fig. 1(b), where two RLC circuits [i.e., the left circuit

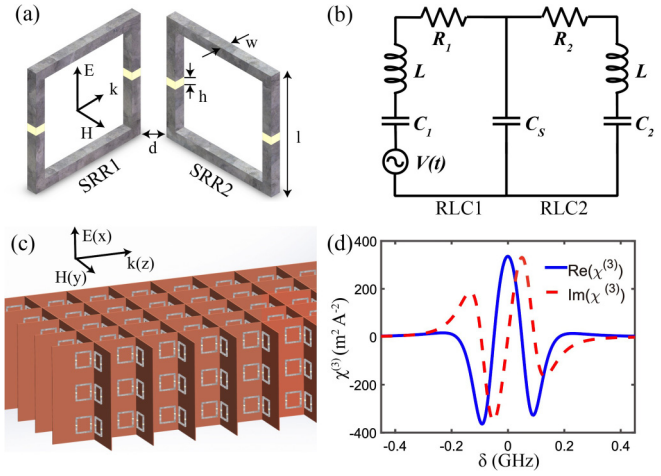

FIG. 1. (a) Metamaterial element (magnetic meta-atom) designed to obtain large magnetic responses, where two varactor-loaded SRR1 and SRR2 are arranged to be perpendicular to each other. Propagation direction of the incident radiation is chosen to make the SRR1 (SRR2) perform as a bright (dark) magnetic oscillator. Dimensions of the two SRRs are $l = 8$ mm, $w = 0.5$ mm, and $h = 0.2$ mm. (b) RLC-circuit analog of the meta-atom, with the left circuit RLC1 (right circuit RLC2) representing SRR1 (SRR2). (c) Schematic of the PIT metamaterial consisting of a periodic array of magnetic meta-atoms. Inset shows the coordinate system indicating the electric field **E**, magnetic field **H**, and wave vector **k**, which are respectively along the x, y, and z directions. (d) Giant magnetic Kerr nonlinearity of the metamaterial working under PIT condition. Real part [i.e., Re($\chi^{(3)}$), with the value up to 385 m^2 A^{-2} near $\delta = 0$] and imaginary part [i.e., Im($\chi^{(3)}$), with vanishing value near $\delta = 0$] of the third-order nonlinear magnetic susceptibility $\chi^{(3)}$ as functions of the frequency detuning δ. The system parameters used are given in the text.

RLC1 (bright oscillator) and the right circuit RLC2 (dark oscillator)] have their capacitance, resistance, and inductance respectively given by C_1, R_1, L_1 and C_2, R_2, L_2, with one shared capacitance C_s (for simplicity $L_1 = L_2 = L$ is assumed in our consideration). The external excitation is described by the electromotive voltage $V(t)$ induced by the incident radiation field. The capacitance C_1 (C_2) is a function of the voltage across the SRR1 (SRR2), which is nonlinear due to the insertion of the varactors (see Appendix A for detail).

Introducing renormalized voltage [13] $q_\alpha = Q_\alpha/C_0$ [$\alpha = 1, 2$; C_0 is the capacitance value in the linear regime for both the capacitances C_1 and C_2, $Q_\alpha = \int_0^t I_\alpha(t')dt'$ is the charge with I_α being the electric current in circuit α] and applying the Kirchhoff voltage law, we obtain the equations of motion

$$\ddot{q}_1 + \gamma_1\dot{q}_1 + \omega_0^2 q_1 - \Omega^2 q_2 + \alpha_1 q_1^2 + \beta_1 q_1^3 = \omega_1^2 V(t), \tag{1a}$$

$$\ddot{q}_2 + \gamma_2\dot{q}_2 + (\omega_0 + \Delta)^2 q_2 - \Omega^2 q_1 + \alpha_2 q_2^2 + \beta_2 q_2^3 = 0, \tag{1b}$$

where γ_1 and γ_2 are respectively the damping rates of q_1 (the bright oscillator) and q_2 (the dark oscillator), Ω^2 is the coupling coefficient between SRR1 and SRR2, ω_1^2 is the coupling coefficient between the bright mode and the external magnetic field, ω_0 ($\approx$5.63 GHz) and $\omega_0 + \Delta$ (Δ is frequency detuning) are respectively the resonance (natural) frequencies of the

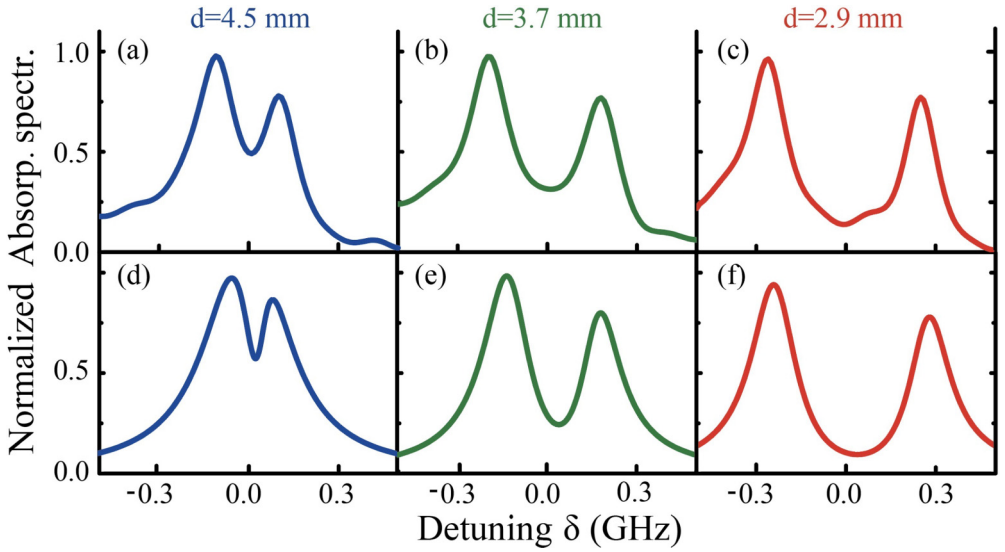

FIG. 2. Linear absorption spectrum of the magnetic PIT metamaterial. Panels (a)–(c) are numerical results of the linear absorption spectrum [i.e., the imaginary part Im(K) of the linear dispersion relation $K = K(\delta)$] versus the frequency detuning δ for different separations (between the two SRRs) $d = 4.5$, 3.7, and 2.9 (in mm), respectively. Panels (d)–(f) are the corresponding analytical results based on Eq. (6) obtained by solving model (1) in the linear regime.

bright and dark oscillators, α_α and β_α ($\alpha = 1, 2$) represent respectively the second-order and third-order nonlinear coefficients (contributed by the varactors). A detailed derivation of model (1a), (1b) and explicit expressions of γ_1, γ_2, ω_0, ω_1, Ω, α_1, α_2, β_1, and β_2 are given in Appendix A.

III. RESULTS AND DISCUSSION

A. Numerical result for linear magnetic excitations

To support our analytical approach given below, a numerical simulation of the linear magnetic response of the system based on the Maxwell equations is carried out first. Figures 2(a)–2(c) illustrate the results of the normalized linear absorption spectrum Im(K) as a function of the frequency detuning δ respectively for d (the separation between the two SRRs) taken to be 4.5, 3.7, and 2.9 mm, obtained numerically by using a commercial finite difference time-domain software package (CST Microwave Studio). In our simulation, periodic boundary conditions are adopted and the substrate is assumed to be made of a FR4 circuit board material [15] with dielectric constant $\epsilon = 4.4(1 + 0.02i)$; a perfect electric conductor is assumed for the metal, whose loss is partially included into the complex dielectric constant of the metamaterial [37]. A standard retrieval procedure is employed for finding the frequency-dependent constitutive parameters of the metamaterial based on the transmission and reflection coefficients of metamaterial elements. The damping rates γ_1, γ_2, and the resonance frequency ω_0 in the model Eqs. (1a) and (1b) are obtained by fitting the numerical result [i.e., Figs. 2(a)–2(c)] and the analytical one given in the next section [i.e., Figs. 2(d)–2(f)] on the linear absorption spectrum of the metamaterial.

From Fig. 2, we see that a PIT transparency window opens in the absorption spectrum; moreover, the PIT transparency window becomes wider and deeper when d decreases. The physical reason for the occurrence of the PIT transparency window is due to the destructive interference between the bright and dark oscillators, which can be controlled actively by changing the separation d between the two SRRs.

B. Analytical result on linear magnetic excitations

To acquire a deep understanding of the physical property of the system, we now consider the linear and nonlinear magnetic response by using an analytical approach. Note that, when the two SRRs are arranged in the manner shown in Fig. 1(a), the electric-dipole moments contributed by the two SRRs in the meta-atom cancel each other. As a result, not only the meta-atom [Fig. 1(a)] but also the whole metamaterial [Fig. 1(c)] exhibit a predominantly magnetic response to the external radiation field [3,15]. In this situation, the radiation dynamics of the system is governed by the equation of motion for the magnetic field $\mathbf{H}$, given by

$$\nabla^2\mathbf{H} - \frac{1}{c^2}\frac{\partial^2\mathbf{H}}{\partial t^2} = \frac{1}{c^2}\frac{\partial^2\mathbf{M}}{\partial t^2}, \tag{2}$$

where $\mathbf{M} = \chi_D^{(1)}\mathbf{H} - N_0 S C_0(\partial q_1/\partial t)\mathbf{e}$ is the magnetic polarization intensity, with $\chi_D^{(1)}$ being the magnetic susceptibility of the background material (i.e., the substrate, which is assumed to be linear), N_0 the meta-atom density, S the area of the SRRs, and $\mathbf{e}$ the direction of the magnetic moment contributed by the bright oscillator SRR1. Note that, due to the fact that the dark oscillator SRR2 can only be excited through its coupling to the bright oscillator SRR1, and that the direction of the radiation field at the dark oscillator SRR2 is perpendicular to the magnetic polarization, the contribution of the dark oscillator SRR2 to the magnetic polarization intensity is very small and hence can be safely neglected. In addition, when obtaining Eq. (2) a magnetic-dipole approximation is used; this is reasonable because the wavelength of the incident radiation field (≈100 mm) is much larger than the thickness

of the meta-atom (≈1 mm), and hence the radiation field seen by the meta-atom is nearly homogeneous.

We employ a method of multiple scales [30,31,38–40] to analytically solve the nonlinear magnetic oscillator Eq. (1) and the Maxwell Eq. (2). We assume the incident radiation has frequency ω_f (which is near the resonance frequency ω_0 of the SRRs), and take $q_\alpha = q_{d\alpha} + [q_{f\alpha}e^{i(k_0z-\omega_0t)} + \text{c.c.}] + [q_{s\alpha}e^{2i(k_0z-\omega_0t)} + \text{c.c.}] + [q_{t\alpha}e^{3i(k_0z-\omega_0t)} + \text{c.c.}]$, $H = H_d + [H_f e^{i(k_f z-\omega_f t)} + \text{c.c.}] + [H_s e^{i(k_s z-\omega_s t)} + \text{c.c.}] + [H_t e^{i(k_t z-\omega_t t)} + \text{c.c.}]$. Here "c.c." means complex conjugate; $q_{d\alpha}$, $q_{f\alpha}$, $q_{s\alpha}$, and $q_{t\alpha}$ are respectively the amplitudes of the longwave (rectification field), shortwave (fundamental wave), second-harmonic wave, and third-harmonic waves of the oscillator α ($\alpha = 1, 2$), with k_0 (ω_0) being the wave number (frequency) of the fundamental wave; H_d, H_f, H_s, and H_t are respectively the amplitudes of the longwave, shortwave, second-harmonic wave, and third-harmonic waves of the magnetic field. By using the rotating-wave and slowly varying envelope approximations, from Eqs. (1) and (2) we can obtain a series of equations for $q_{\mu\alpha}$ and H_μ ($\mu = d, f, s, t$) (see Appendix B).

Take the asymptotic expansion $q_{f\alpha} = \lambda q_{f\alpha}^{(1)} + \lambda^2 q_{f\alpha}^{(2)} + \lambda^3 q_{f\alpha}^{(3)} + \cdots$, $q_{d\alpha} = \lambda^2 q_{d\alpha}^{(2)} + \lambda^3 q_{d\alpha}^{(3)} + \cdots$, $q_{s\alpha} = \lambda^2 q_{s\alpha}^{(2)} + \lambda^3 q_{s\alpha}^{(3)} + \cdots$, $q_{t\alpha} = \lambda^3 q_{t\alpha}^{(3)} + \cdots$, $H_f = \lambda H_f^{(1)} + \lambda^2 H_f^{(2)} + \lambda^3 H_f^{(3)} + \cdots$, where λ is a small dimensionless parameter characterizing the amplitude of the incident magnetic field. All quantities on the right-hand side of the expansion are assumed as functions of the multiscale variables $x_1 = \lambda x$, $y_1 = \lambda y$, $z_j = \lambda^j z$ ($j = 0, 1, 2$), and $t_j = \lambda^j t$ ($j = 0, 1$). Substituting this expansion into the equations for $q_{\mu j}$ and H_μ and comparing powers of λ, we obtain a chain of linear but inhomogeneous equations (see Appendix C), which can be solved order by order.

At the first-order we obtain the solution for the shortwave field

$$H_f^{(1)} = F\exp[i(Kz_0 - \delta t_0)], \tag{3}$$

$$q_{f1}^{(1)} = -\frac{ig\omega_0 D_2(\delta)H_f^{(1)}}{D_1(\delta)D_2(\delta) - \Omega^4}, \tag{4}$$

$$q_{f2}^{(1)} = -\frac{ig\omega_0\Omega^2 H_f^{(1)}}{D_1(\delta)D_2(\delta) - \Omega^4}. \tag{5}$$

Here F is a yet to be determined envelope function depending on the slow variables x_1, y_1, z_1, z_2, t_1; $\delta = \omega_f - \omega_0$ is the frequency detuning; and K is linear dispersion relation, given by

$$K = \frac{n_D}{c}\delta + \frac{\kappa_0 g\omega_0 D_2(\delta)}{D_1(\delta)D_2(\delta) - \Omega^4}, \tag{6}$$

where $D_j(l\delta) = \omega_0^2 - l^2(\omega_0+\delta)^2 - il\gamma_j(\omega_0+\delta)$ ($j, l = 1, 2$), $\kappa_0 = N_0 S C_0\omega_0^2/(2cn_D)$, $n_D = (1+\chi_D^{(1)})^{1/2}$, and $g = \mu_0\omega_1^2 S$ (μ_0 is the vacuum permeability).

Shown in Figs. 2(d)–2(f) are the normalized absorption spectrum Im(K) (i.e., the imaginary part of K) as a function of δ for the separation between the two SRRs $d = 4.5$, 3.7, and 2.9 (in mm), respectively. Comparing with the upper and lower parts of Fig. 2, we see that the analytical result on the PIT spectrum and the related transparency windows based on Eqs. (1) and (2) (the lower part of the figure) agrees quite well with the one based on the numerical simulation using CST Microwave Studio (the upper part of figure). When plotting the figure by using Eq. (6), the system parameters used are obtained by fitting the numerical result, which are given as follows: damping rates are $\gamma_1 \approx 0.2602$ GHz and $\gamma_2 \approx 0.071$ GHz; the parameter of the coupling strength between SRR1 and SRR2 (i.e., Ω) is varied from 0.7 to 1.7 GHz (corresponding to the variation of d from 4.5 to 2.9 mm).

To obtain a clear understanding of the variation of the width of the transparency window for different d and of the character of the interference between the bright and dark oscillators, we make a spectrum decomposition (based on the method developed in Ref. [38]) on the absorption spectrum Im(K) for different coupling strength Ω^2 between the bright and dark oscillators, which can be divided into the following regimes:

(i) PIT regime. This is a weak absorption regime occurring in the case of weak coupling for $\Omega^2 < (\gamma_1 - \gamma_2)\omega_0/2$. The absorption spectrum Im(K) in this regime can be decomposed to the sum of two Lorentzians terms:

$$\text{Im}(K) = \frac{GC_+W_+}{\delta^2 + W_+^2} - \frac{GC_-W_-}{\delta^2 + W_-^2}, \tag{7}$$

where $W_\pm = -(\gamma_1+\gamma_2)/4 \pm [(\gamma_1-\gamma_2)^2/16 - T^2]^{\frac{1}{2}}$, $T = \Omega^2/(2\omega_0)$, and $C_\pm = \pm(\gamma_2/2 + W_\pm)/[(\gamma_1-\gamma_2)^2/4 - 4T^2]^{\frac{1}{2}}$. Illustrated in Fig. 3(a) is Im(K) as a function of δ for $\Omega = 0.7$ GHz, where the dashed (dotted-dashed) curve shows the result of the first (second) Lorentzian term, which takes a negative (positive) value. Because of the destructive interference between bright (SRR1) and dark (SRR2) oscillators, the superposition of the two curves results in the appearance of a small dip in Im(K) curve (i.e., the solid line), a typical character of PIT.

(ii) PIT-ATS crossover regime. This regime occurs in the case of intermediate coupling where $\Omega^2 > (\gamma_1 - \gamma_2)\omega_0/2$. In this regime, the spectrum decomposition gives

$$\begin{aligned}\text{Im}(K) = &\frac{G(\gamma_1+\gamma_2)/8}{(\delta-\delta_0)^2 + (\gamma_1+\gamma_2)^2/16} \\ &+ \frac{G(\gamma_1+\gamma_2)/8}{(\delta+\delta_0)^2 + (\gamma_1+\gamma_2)^2/16} \\ &- \frac{GJ(\delta-\delta_0)}{(\delta-\delta_0)^2 + (\gamma_1+\gamma_2)^2/16} \\ &+ \frac{GJ(\delta+\delta_0)}{(\delta+\delta_0)^2 + (\gamma_1+\gamma_2)^2/16},\end{aligned} \tag{8}$$

where $\delta_0 = [T^2 - (\gamma_1-\gamma_2)^2/16]^{1/2}$ and $J = (\gamma_2-\gamma_1)/(8\delta_0)$. One sees that Im($K$) consists of four terms. The first two terms are Lorentzians that give two resonance peaks belonging to the SRR1 and the SRR2, respectively. The dip between the two Lorentzian peaks is a frequency gap between two resonances, a typical character of Autler-Townes splitting (ATS). However, the third and fourth terms (which are interference terms) lower significantly the dip formed by the first two terms, giving the system some characteristics of PIT. Since both the PIT and the ATS occur simultaneously, such a phenomenon is called a PIT-ATS crossover [38]. Illustrated in Fig. 3(b) are

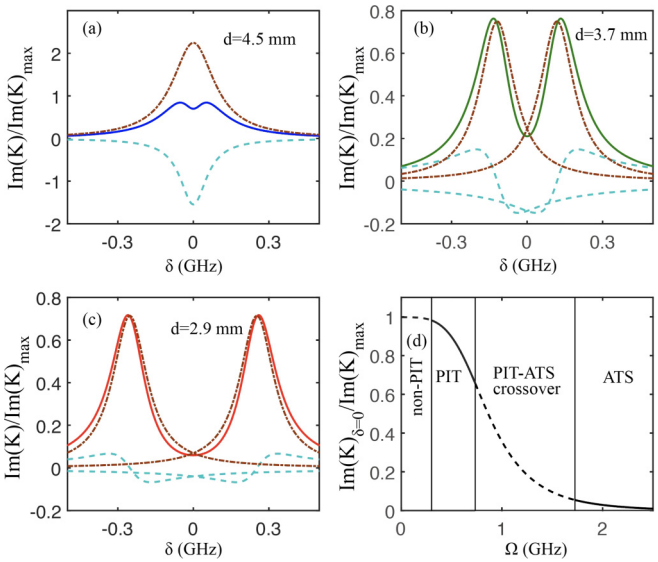

FIG. 3. Crossover from PIT to Autler-Towns splitting (ATS). (a) The dashed (dotted-dashed) curve is the result of the first (second) Lorentzian term in Eq. (7) as a function of detuning δ. The solid curve is the absorption spectrum $\mathrm{Im}(K)$ in the weak-coupling (PIT) regime ($d = 4.5$ mm). (b) The dashed-dotted lines are results of the first two Lorentzian terms in Eq. (8); the dashed lines are results of the third and fourth terms in Eq. (8). The solid line is the sum of all the four terms, which gives $\mathrm{Im}(K)$ curve in the intermediate coupling (PIT-ATS crossover) regime ($d = 0.37$ mm). (c) The same as panel (b) but with $d = 2.9$ mm, giving $\mathrm{Im}(K)$ in the strong-coupling (ATS) regime. (d) A "phase" diagram shows the transition from PIT to ATS when the coupling strength Ω^2 is varied, where a non-PIT (strong absorption) regime for very small Ω^2 is also plotted (leftmost side).

results of various terms in Eq. (8) and the total absorption spectrum $\mathrm{Im}(K)$ for $\Omega = 1.2$ GHz.

(iii) ATS regime. It appears for the case of strong coupling where $\Omega^2 \gg (\gamma_1 - \gamma_2)\omega_0/2$. The spectrum decomposition of $\mathrm{Im}(K)$ in this regime is still given by Eq. (8), but the destructive interference effect contributed by the last two terms plays a negligible role. Shown in Fig. 3(c) are results for $\Omega = 1.7$ GHz. One sees that, in this strong-coupling regime, the absorption spectrum curve $\mathrm{Im}(K)$ displays mainly the character of ATS.

Figure 3(d) shows the phase diagram from PIT to ATS for different coupling strengths Ω^2, where three regimes (i.e., PIT, PIT-ATS crossover, and ATS) are indicated clearly. For completeness, a non-PIT regime (or called as strong absorption regime), where radiation absorption is strong, occurring in the case of very weak coupling [i.e., $\Omega^2 \ll (\gamma_1 - \gamma_2)\omega_0/2$], is also plotted; see the leftmost side of the figure.

C. Nonlinear envelope equation and giant magnetic Kerr nonlinearity

To reveal the nonlinear propagation property of the radiation field, we need to investigate the solution to Eqs. (1) and (2) at high-order approximations. Based on the linear (first-order) solution obtained above, we find that, at the second-order approximation, the envelope function F satisfies the equation $i[\partial F/\partial z_1 + (1/V_g)\partial F/\partial t_1] = 0$, with $V_g = (\partial K/\partial\delta)^{-1}$ being the group velocity of the envelope. Explicit expressions for solutions $q^{(2)}_{\mu\alpha}$ and $H^{(2)}_{\mu}$ at this order are presented in Appendix C.

With these results, we can go to third-order approximation. A solvability condition yields another envelope equation for F, which, combined with the envelope equation obtained from the second-order approximation, has the form

$$i\frac{\partial F}{\partial z_2} - \frac{1}{2}K_2\frac{\partial^2 F}{\partial \tau_1^2} + \frac{c}{2\omega_0 n_D}\left(\frac{\partial^2}{\partial x_1^2} + \frac{\partial^2}{\partial y_1^2}\right)F + \frac{\omega_0}{2cn_D}\chi^{(3)}|F|^2 F e^{-2\bar{\alpha}z_2} = 0. \tag{9}$$

Here $\tau_1 = \epsilon(t - z/V_g)$; $K_2 = \partial^2 K/\partial\delta^2$ is the coefficient describing the group-velocity dispersion; the second term $\frac{c}{2\omega_0 n_D}(\frac{\partial^2}{\partial x_1^2} + \frac{\partial^2}{\partial y_1^2})F$ describes diffraction effect; $\bar{\alpha} = \lambda^{-2}\mathrm{Im}(K)$ is the coefficient describing linear absorption (which is small due to the PIT effect illustrated above); $\chi^{(3)}$ is the third-order nonlinear magnetic susceptibility that results from the self-phase modulation, with the expression given by

$$\chi^{(3)} = \frac{-iN_0 S\omega_0 C_0}{D_1(\delta)D_2(\delta) - \Omega^4}\left\{2\alpha_1^2 g^2\omega_0^2 D_2(\delta)\left[\frac{D_2(\delta)^2 D_2(2\delta)E_1^*}{A} - \frac{2\omega_0^2|D_2(\delta)|^2 E_1}{B}\right]\right.$$
$$+2\alpha_1\alpha_2 g^2\omega_0^2\Omega^4\left[\frac{D_2(\delta)\Omega^2 E_1^* + D_2(\delta)^2 E_2^*}{A} - \frac{2D_2(\delta)^2\Omega^2 E_1 + 2|D_2(\delta)|^2 E_2}{B}\right]$$
$$\left.+2\alpha_2^2 g^2\omega_0^2\Omega^6\left[\frac{D_1(2\delta)E_2^*}{A} - \frac{\omega_0^2 E_2}{B}\right] + 3D_2(\delta)\beta_1|E_1|^2 E_1) + 3\Omega^2\beta_2|E_2|^2 E_2\right\}. \tag{10}$$

Here $A=[D_1(2\delta)D_2(2\delta)-\Omega^4][D_1(\delta)D_2(\delta)-\Omega^4]^2$, $B=(\omega_0^4-\Omega^4)|D_1(\delta)D_2(\delta)-\Omega^4|^2$, $E_1 = -[ig\omega_0 D_2(\delta)]/[D_1(\delta)D_2(\delta)-\Omega^4]$, and $E_2 = -[ig\omega_0\Omega^2]/[D_1(\delta)D_2(\delta)-\Omega^4]$. The explicit derivation of Eqs. (9) and (10) are presented in Appendix C. One sees that $\chi^{(3)}$ is proportional to the parameters α_1, α_2, β_1, and β_2, which means that they are contributed by the quadratic and cubic nonlinear terms in Eq. (1) (originated by the nonlinear property of the varactors inserted in the gaps of the SRRs).

Shown in Fig. 4 are curves of the real part of the third-order nonlinear magnetic susceptibility $\chi^{(3)}$ (i.e., $\mathrm{Re}[\chi^{(3)}]$; solid red line) and the imaginary part of linear magnetic susceptibility $\chi^{(1)}$ (i.e., $\mathrm{Im}[\chi^{(1)}]$; dashed blue line) as functions of the coupling strength Ω, for four different coupling (i.e., non-PIT,

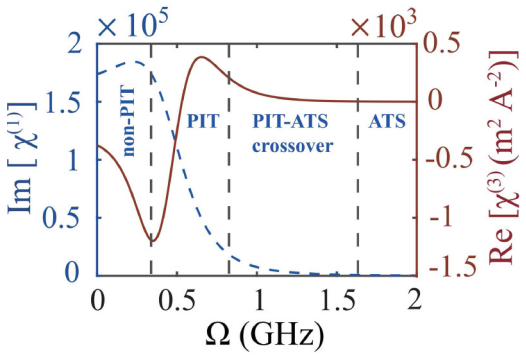

FIG. 4. Giant magnetic Kerr nonlinearity of the PIT metamaterial. The real part of the third-order nonlinear magnetic susceptibility $\chi^{(3)}$ (i.e., $\mathrm{Re}[\chi^{(3)}]$; solid red line) and the imaginary part of the linear magnetic susceptibility (i.e., $\mathrm{Im}[\chi^{(1)}]$; dashed blue line), as functions of the coupling strength Ω for $S = 5 \times 10^{-5}$ m^2, $C_0 = 1.6$ pF, $V_p = 1.5$ V, and $M = N = 0.8$ (other system parameters used have been given in the text). Four different regimes (i.e., non-PIT, PIT, PIT-ATS, and ATS regimes) are indicated which occur as Ω is increased.

PIT, PIT-ATS, and ATS) regimes. The system parameters used for plotting the figure are $S = 5 \times 10^{-5}$ m^2, $C_0 = 1.6$ pF, $V_p = 1.5$ V, $M = N = 0.8$, $\kappa_0 = 2.817$ m^{-4} kg^{-1} s^3 A^2, and $\delta = 0.05$ GHz. Values of the nonlinear parameters are derived to be $\alpha_1 = \alpha_2 = -0.2667$ V^{-1} and $\beta_1 = \beta_2 = 0.0356$ V^{-2}. From the figure, we can obtain the following conclusions:

(i) For $\Omega = 0$ (for which the dark oscillator plays no role, i.e., the system works in the non-PIT regime), $\mathrm{Re}[\chi^{(3)}]$ can reach the value of -569 m^2 A^{-2}, which agrees with the result of previous work by Poutrina *et al.* [15] for the magnetic metamaterial with each meta-atom containing only a single SRR. However, in this strong absorption regime the linear absorption $\mathrm{Im}[\chi^{(1)}]$ is also quite large, which hinders most practical applications for radiation propagations.

(ii) In the PIT region, the linear absorption (i.e., $\mathrm{Im}[\chi^{(1)}]$) can be largely eliminated (for convenience in the figure the crossover from the non-PIT regime to the PIT regime is indicated by a vertical black dashed line). Except for this, the real part of the nonlinear magnetic susceptibility (i.e., $\mathrm{Re}[\chi^{(3)}]$) can reach to a very large value. For example, for $\Omega = 0.89$ GHz we obtain

$$\mathrm{Re}[\chi^{(3)}] = 3.85 \times 10^2 \ \mathrm{m}^2\,\mathrm{A}^{-2}. \tag{11}$$

At the same time, the imaginary part of nonlinear magnetic susceptibility (i.e., $\mathrm{Im}[\chi^{(3)}]$) may be made very small [see Fig. 1(d), where $\mathrm{Re}[\chi^{(3)}]$ and $\mathrm{Im}[\chi^{(3)}]$ are plotted as functions of the frequency detuning δ]. Note that the value given in Eq. (11) is equivalent to 2.4×10^6 in units of esu. Thus the third-order nonlinear magnetic susceptibility in the present PIT system is 16 orders of magnitude larger than those obtained by using conventional magnetic materials, where the typical value is given by $\chi^{(3)} \approx 2.5 \times 10^{-10}$ esu [41]. The physical reason for such a large third-order magnetic Kerr nonlinearity obtained in our system is due to the fact that the magnetic field **H** is resonant with the bright and dark oscillators q_1, q_2 and the system works under the PIT condition. Interestingly, the sign of $\mathrm{Re}[\chi^{(3)}]$ flips from negative to positive around $\Omega = 0.53$ GHz, which means that the magnetic Kerr nonlinearity of the system may experience a transition from self-defocusing to self-focusing, which is promising for practical applications based on pure magnetic nonlinear responses.

(iii) In the PIT regime, the value of $\mathrm{Re}[\chi^{(3)}]$ may acquire its largest enhancement near the transition point between the non-PIT (strong absorption) regime and the PIT regime, i.e., $\mathrm{Re}[\chi^{(3)}] \approx -12.0 \times 10^2$ m^2 A^{-2} for $\Omega = 0.351$ GHz. However, this enhancement accompanies a very large linear absorption (i.e., $\mathrm{Im}[\chi^{(1)}]$ is also large), thus it is not applicable for low-loss radiation propagation.

(iv) For larger Ω, the system works in the intermediate-coupling (i.e., PIT-ATS) regime, where $\mathrm{Im}[\chi^{(1)}]$ is suppressed significantly by the dark oscillator but $\mathrm{Re}[\chi^{(3)}]$ is also decreased. By increasing large Ω further, the system enters into the strong-coupling (i.e., ATS) regime, for which $\mathrm{Im}[\chi^{(1)}]$ can be completely suppressed by the dark oscillator; however, $\mathrm{Re}[\chi^{(3)}]$ tends to vanish, and thus is not useful for realizing large magnetic Kerr nonlinearity.

From these results obtained from the non-PIT, PIT, PIT-ATS, and ATS regimes obtained for different Ω (i.e., from the very-weak-coupling to the strong-coupling regimes), we see that there is a trade-off between the suppression of large absorption and the acquirement of large Kerr nonlinearity in the system. Only in the weak-coupling PIT regime does the system supports large Kerr nonlinearity and small absorption simultaneously.

IV. ULTRASLOW AND LOW-POWER MAGNETIC SOLITONS

We now turn to consider the formation and propagation of nonlinear magnetic pulses in the system. For simplicity, we focus on the regime where the transverse spatial distribution of radiation is large enough so that the diffraction effect (i.e., the dependence on the transverse coordinates x and y) can be neglected. In this case, the nonlinear envelope equation [i.e., Eq. (9)] reduces to the nonlinear Schrödinger equation,

$$i\left(\frac{\partial}{\partial z} + \alpha_m\right)U - \frac{1}{2}K_2\frac{\partial^2 U}{\partial \tau^2} - W|U|^2U = 0, \tag{12}$$

when returning to the original variables, where $W = -[\omega_0/(2cn_D)]\chi^{(3)}$, $\tau = t - z/V_g$, $\alpha_m = \lambda^2\bar{\alpha}$, and $U = \lambda F \exp(-\alpha_m z)$. Generally, Eq. (12) has complex coefficients and hence is a Ginzburg-Landau equation. However, due to the PIT effect, the imaginary part of the complex coefficients can be made much smaller than their real part. When converted into the dimensionless form, Eq. (12) becomes

$$i\frac{\partial}{\partial s}u + \frac{1}{2}\frac{\partial^2 u}{\partial \sigma^2} + |u|^2u = id_0u, \tag{13}$$

with $z = -L_D s$, $\tau = \tau_0\sigma$, $U = U_0 u$, and $d_0 = L_D/L_A$. Here τ_0, $L_D \equiv \tau_0^2/\tilde{K}_2$, $L_A \equiv 1/\alpha_m$, and $U_0 \equiv (1/\tau_0)(\tilde{K}_2/\tilde{W})^{1/2}$ are respectively typical pulse length, dispersion length, absorption length, and pulse amplitude (the tilde symbol means taking real part). Notice that, in order to form solitons, L_D has been set to equal typical nonlinearity length, defined by L_{NL} [$\equiv 1/(U_0^2\tilde{W})$].

If d_0 is small (this is the case we have here due to the PIT effect), the term $d_0 u$ can be taken as a perturbation. One can use a perturbation method to solve the Eq. (13) to obtain single and multiple soliton solutions [42]. The single bright soliton solution is given by $u = \eta\ \mathrm{sech}[2\eta e^{d_0 s}(\sigma - \sigma_0 + 4\varsigma s)]e^{-2i\varsigma\sigma - 4i(\varsigma^2-\eta^2)s + d_0 s - i\phi_0}$, where η, ς, σ_0, and ϕ_0 are real free parameters determining the amplitude (as well as the width), propagating velocity, initial position, and initial phase of the soliton, respectively. When taking $\eta = 1/2$, $\varsigma = \sigma_0 = \phi_0 = 0$, and noting that $s = -z/L_{\mathrm{D}}$, we obtain the expression of the magnetic field corresponding the single-soliton solution

$$H = \frac{1}{\tau_0}\sqrt{\frac{\widetilde{K}_2}{\widetilde{W}}}\ \mathrm{sech}\left[\frac{1}{\tau_0}\left(t - \frac{z}{\widetilde{V}_g}\right)\right]e^{i\phi(z,t) - z/L_A} + \mathrm{c.c.}, \quad (14)$$

with $\phi(z,t) \equiv [\widetilde{K} + k_f - 1/(L_D)]z - w_f t$, which describes a localized nonlinear magnetic pulse with velocity $\widetilde{V}_g$ and a small damping during propagation.

For $\delta = 0.1$ GHz and with the other parameters given above, we obtain numerical values of the coefficients in Eq. (12), given by $\alpha_m = 0.051\ \mathrm{cm}^{-1}$, $K_2 = (4.1 + 0.12i) \times 10^{-17}\ \mathrm{cm}^{-1}\ \mathrm{s}^2$, and $W = (5.2 + 0.13i) \times 10^5\ \mathrm{cm\,A}^{-2}$. We see that, as expected, the imaginary part of these coefficients are indeed much smaller than their real part. By taking $\tau_0 = 1 \times 10^{-9}$ s, we obtain $U_0 = 8.9 \times 10^{-3}\ \mathrm{cm}^{-1}\,\mathrm{A}^{-1}$, $L_{\mathrm{D}} = L_{\mathrm{NL}} = 2.4 \times 10^{-2}$ cm, and $L_{\mathrm{A}} = 19.6$ cm. Thus one has $d_0 = 1.2 \times 10^{-3}$ and hence the dissipation in the system can be indeed taken as a perturbation.

The power associated with the magnetic soliton is given by Poynting's vector integrated over the cross section of the radiation in the transverse directions, i.e., $P = \int(\mathbf{E} \times \mathbf{H}) \cdot \mathbf{e}_z dS$, where $\mathbf{e}_z$ is the unit vector along the propagation (i.e., z) direction. Substituting the expressions of $\mathbf{H}$ and $\mathbf{E}$ into P, we obtain the peak power of the soliton, given by $\tilde{P}_{\max} = 2\mu_0 c n_p S\widetilde{K}_2/(\widetilde{W}\tau_0^2)$. Here $n_p = 1 + c\widetilde{K}/\omega_0$ is the refractive index and S_0 is the area of the intensity distribution of the radiation field in the transverse directions. Using the above parameters and taking $S = 5 \times 10^{-5}\ \mathrm{m}^2$, the peak power for generating the soliton is found to be

$$\tilde{P}_{\max} \simeq 29.7\ \mathrm{mW}, \quad (15)$$

which means that to create such a soliton in the system a very low input power is needed. This is different from conventional media (such as optical fibers), where picosecond or femtosecond laser pulses are required to reach a much high power (usually on the order of several hundred kW or above) to produce enough nonlinearity to form solitons.

Based on the system parameters given above, the group velocity of the magnetic soliton is estimated to be

$$\tilde{V}_g \simeq 7.3 \times 10^{-3} c, \quad (16)$$

which is much smaller than the light speed c in vacuum. From Eqs. (15) and (16), we see that the magnetic soliton obtained in the present magnetic PIT system has ultraslow propagation velocity and ultraslow generation power, which is also different from those obtained in conventional magnetic metamaterials considered before [43–45].

To test the stability of the magnetic soliton in the PIT system, a numerical simulation is carried out. Shown in Fig. 5(a) is the result of the dimensionless radiation intensity $|H/U_0|^2$ of the magnetic soliton as a function of dimensionless time t/τ_0 and dimensionless distance z/L_{D}. The solution is obtained by numerically solving Eq. (12) with the complex coefficients taken into account, with the initial condition given by $H(0,t)/U_0 = \mathrm{sech}(t/\tau_0)$. We see that the shape of the soliton undergoes no apparent deformation during propagation.

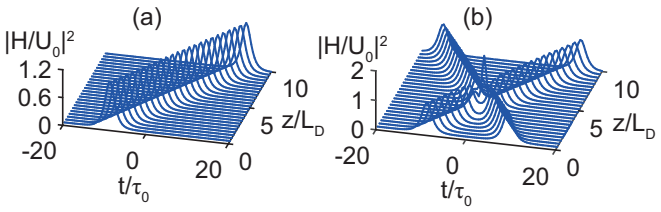

FIG. 5. Ultraslow and low-power magnetic solitons and their interaction in the PIT metamaterial. (a) Propagation of the magnetic soliton by taking the dimensionless intensity $|H/U_0|^2$ as a function of t/τ_0 and z/L_D. (b) Collision between two magnetic solitons.

The collision between two magnetic solitons is also investigated numerically, with the result shown in Fig. 5(b). In the simulation, the initial condition used is $H(0,t)/U_0 = \mathrm{sech}[(t-3.0)/\tau_0] + 1.2\mathrm{sech}[1.2(t+3.0)/\tau_0]$. We see that the both solitons can resume their original shapes after the collision, indicating that solitons in the PIT-metamaterial are robust during interaction.

V. SUMMARY

In this work, we have presented a scheme for realizing strong, low-loss, and pure magnetic responses both in the linear and nonlinear regimes by using a metamaterial constructed by an array of meta-atoms consisting of two coupled VLSRRs working under the condition of PIT. We have demonstrated that the PIT in such metamaterial can not only significantly suppress radiation absorption but also greatly enhance the magnetic Kerr nonlinearity, which may be many orders of magnitude larger than those obtained by conventional magnetic materials reported up to now. Based on such new nonlinear metamaterial, we have further demonstrated that stable magnetic solitons with ultraslow propagation velocity and very low generation power can be generated in the system. Our research opens an avenue for the design of novel metamaterial devices with strong, low-loss, pure, and actively tunable magnetic responses and for the realization of stable and low-power nonlinear magnetic pulses, which is promising for applications in information processing and transmission.

ACKNOWLEDGMENTS

This work was supported by the National Science Foundation of China (19975098, 11174080, 11847221, 11904104), the Shanghai Sailing Program (18YF1407100), the China Postdoctoral Science Foundation (2017M620140), and the International Postdoctoral Exchange Fellowship Program (20180040).

APPENDIX A: DERIVATION OF THE COUPLED NONLINEAR OSCILLATOR EQUATIONS

The geometric structure of the meta-atoms, i.e., the varactor-loaded split-ring resonators (VLSRRs) [13,15], is illustrated in Figure 1(a) of the main text. Each meta-atom can be well modeled as an RLC circuit model with external excitation [as shown in Figure 1(b) of the main text], where two RLC circuits [i.e., RLC1 (bright oscillator) and RLC2 (dark oscillator)] have different capacitance, resistance, and inductance, respectively given by C_1, R_1, L_1 and C_2, R_2, L_2, with one shared capacitance C_S (for simplicity $L_1 = L_2 = L$ is assumed in our consideration). The external excitation (i.e., the incident radiation field) gives an electromotive voltage $V(t) = -\mu_0 S \partial H/\partial t$ (μ_0 is the permeability of vacuum) to the bright oscillator (i.e., the circuit RLC1), which generates currents I_α in the circuit RLC$_\alpha$ ($\alpha = 1, 2$). Based on the formula $C_\alpha \equiv dQ_\alpha/dV_\alpha$ with Q_α (time-dependent charge) $\equiv \int_0^t I_\alpha(t')dt'$ and adopting Kirchhoff voltage law, we obtain the equations of motion

$$L\frac{dI_1}{dt} + R_1 I_1 + \frac{Q_1}{C_S} + V_1 - \frac{Q_2}{C_S} = V(t), \tag{A1a}$$

$$L\frac{dI_2}{dt} + R_2 I_2 + \frac{Q_2}{C_S} + V_2 - \frac{Q_1}{C_S} = 0, \tag{A1b}$$

where $\ddot{I}_\alpha \equiv d^2 I_\alpha/dt^2$, V_1 (V_2) is voltage across the varactor in SRR1 (SRR2).

The nonlinear capacitances (originated from the varactors) in the circuits RLC1 and RLC2 can be respectively described by formulas [13] $C_1 = C_0(1 - V_1/V_p)^{-M}$ and $C_2 = C_0(1 - V_2/V_p)^{-N}$, with C_0 being the value of the capacitance in the linear regime and V_p an intrinsic potential parameter. For simplicity, we assume $M = N$, i.e., the capacitances of the two varactors have the same nonlinear response (which generally can be actively designed and manipulated). We expect that, at a moderate power level, the nonlinear responses of the both varactors are weak, so that C_1 and C_2 can be respectively Taylor expanded as power series of V_1 and V_2, and only the first three terms are kept. Then by introducing the normalized charges $q_\alpha \equiv Q_\alpha/C_0$ ($\alpha = 1, 2$) and taking V_1 and V_2 as functions of q_1 and q_2, we obtain

$$V_1(q_1) \approx q_1 - \frac{M}{2V_P}q_1^2 + \frac{M(2M-1)}{6V_P^2}q_1^3, \tag{A2a}$$

$$V_2(q_2) \approx q_2 - \frac{N}{2V_P}q_2^2 + \frac{N(2N-1)}{6V_P^2}q_2^3. \tag{A2b}$$

By inserting the expression (A2) into Eq. (A1), we obtain equations of motion for q_1 and q_2 as follows:

$$\ddot{q}_1 + \gamma_1\dot{q}_1 + \omega_0^2 q_1 - \Omega^2 q_2 + \alpha_1 q_1^2 + \beta_1 q_1^3 = \omega_1^2 V(t), \tag{A3a}$$

$$\ddot{q}_2 + \gamma_2\dot{q}_2 + (\omega_0 + \Delta)^2 q_2 - \Omega^2 q_1 + \alpha_2 q_2^2 + \beta_2 q_2^3 = 0, \tag{A3b}$$

where γ_1 and γ_2 ($\gamma_\alpha = R_\alpha/L$, $\alpha = 1, 2$) are respectively the damping rates of the bright oscillator q_1 and dark oscillator q_2, $\Omega^2 \equiv 1/(LC_S)$ is the coupling coefficient between the bright and dark oscillators, $\omega_1^2 = 1/(LC_0)$ is the coupling coefficient between the bright oscillator and the external magnetic field, $\omega_0 \equiv (\omega_1^2 + \Omega^2)^{1/2}$ and $\omega_0 + \Delta$ (Δ is frequency detuning) are respectively the natural frequencies of the bright and dark oscillators, $\alpha_1 \equiv -(\omega_1^2 M)/(2V_p)$, $\alpha_2 \equiv -(\omega_1^2 N)/(2V_p)$, $\beta_1 \equiv [\omega_1^2 M(2M-1)]/(6V_p^2)$, and $\beta_2 \equiv [\omega_1^2 N(2N-1)]/(6V_p^2)$ are respectively the second-order and third-order nonlinear coefficients, contributed by the varactors. For simplicity, the frequency detuning Δ will be taken to be zero since the two SRRs are assumed to have the same structure.

APPENDIX B: EQUATIONS OF MOTION FOR VARIOUS FREQUENCY COMPONENTS OF THE BRIGHT AND DARK OSCILLATORS AND THE MAGNETIC FIELD

We assume that the incident radiation has frequency ω_f, which is near ω_0. Thus, there is a resonant interaction between the magnetic field and the bright and dark oscillators q_1 and q_2. To solve such a resonant nonlinear problem analytically, we assume

$$q_\alpha = q_{d\alpha} + [q_{f\alpha}e^{i(k_0 z - \omega_0 t)} + \text{c.c.}] + [q_{s\alpha}e^{2i(k_0 z - \omega_0 t)} + \text{c.c.}] + [q_{t\alpha}e^{3i(k_0 z - \omega_0 t)} + \text{c.c.}], \tag{B1a}$$

$$H = H_d + [H_f e^{i(k_f z - \omega_f t)} + \text{c.c.}] + [H_s e^{i(k_s z - \omega_s t)} + \text{c.c.}] + [H_t e^{i(k_t z - \omega_t t)} + \text{c.c.}]. \tag{B1b}$$

Here $q_{d\alpha}$, $q_{f\alpha}$, $q_{s\alpha}$, and $q_{t\alpha}$ ($\alpha = 1, 2$) are respectively the amplitudes of the longwave (or called the rectification field), shortwave (fundamental wave), second-harmonic wave, and third-harmonic waves of oscillator α, with k_0 (ω_0) being the wave number (frequency) of the fundamental wave. H_d, H_f, H_s, and H_t are respectively the amplitudes of the longwave, shortwave, second-harmonic wave and third-harmonic waves of the magnetic field. By using the rotating-wave and slowly varying envelope approximations, from Eq. (A3) we obtain a series of equations for the motion for $q_{\mu\alpha}$:

$$\ddot{q}_{f1} + (\gamma_1 - 2i\omega_0)\dot{q}_{f1} - i\gamma_1\omega_0 q_{f1} - \Omega^2 q_{f2} + 2\alpha_1(q_{d1}q_{f1} + q_{s1}q_{f1}^*) + 3\beta_1|q_{f1}|^2 q_{f1} = -ig\omega_f H_f e^{i(k_f z - \omega_f t)}, \tag{B2a}$$

$$\ddot{q}_{f2} + (\gamma_2 - 2i\omega_0)\dot{q}_{f2} - i\gamma_2\omega_0 q_{f2} - \Omega^2 q_{f1} + 2\alpha_2(q_{d2}q_{f2} + q_{s2}q_{f2}^*) + 3\beta_2|q_{f2}|^2 q_{f2} = 0, \tag{B2b}$$

$$\ddot{q}_{d1} + \gamma_1\dot{q}_{d1} - \omega_0^2 q_{d1} - \Omega^2 q_{d2} + 2\alpha_1|q_{f1}|^2 = g\frac{\partial H_d}{\partial t_1}, \tag{B2c}$$

$$\ddot{q}_{d2} + \gamma_2\dot{q}_{d2} - \omega_0^2 q_{d2} - \Omega^2 q_{d1} + 2\alpha_2|q_{f2}|^2 = 0 \tag{B2d}$$

$$\ddot{q}_{s1} + (\gamma_1 - 4i\omega_0)\dot{q}_{s1} - \left(3\omega_0^2 + 2i\gamma_1\omega_0\right)q_{s1} - \Omega^2 q_{s2} + \alpha_1 q_{f1}^2 = -ig\omega_s H_s e^{i(k_s z - \omega_s t)}, \tag{B2e}$$

$$\ddot{q}_{s2} + (\gamma_2 - 4i\omega_0)\dot{q}_{s2} - \left(3\omega_0^2 + 2i\gamma_2\omega_0\right)q_{s2} - \Omega^2 q_{s1} + \alpha_2 q_{f2}^2 = 0, \tag{B2f}$$

$$\ddot{q}_{t1} + (\gamma_1 - 6i\omega_0)\dot{q}_{t1} - \left(8\omega_0^2 + 3i\gamma_1\omega_0\right)q_{t1} - \Omega^2 q_{t2} + \beta_1 q_{f1}^3 = -ig\omega_t H_t e^{i(k_t z - \omega_t t)}, \tag{B2g}$$

$$\ddot{q}_{t2} + (\gamma_2 - 6i\omega_0)\dot{q}_{t2} - \left(8\omega_0^2 + 3i\gamma_2\omega_0\right)q_{t2} - \Omega^2 q_{t1} + \beta_2 q_{f2}^3 = 0, \tag{B2h}$$

with $g = \mu_0\omega_1^2 S$ (μ_0 is the vacuum permeability). Under the slowly varying envelope approximation, the Maxwell Eq. (2) in the main text is converted into the form

$$i\left(\frac{\partial}{\partial z} + \frac{n_D}{c}\frac{\partial}{\partial t}\right)H_f + \frac{c}{2\omega_0 n_D}\nabla_\perp^2 H_f + i\kappa_0 q_{f1} = 0, \tag{B3a}$$

where $\nabla_\perp^2 = \partial^2/\partial x^2 + \partial^2/\partial y^2$, the coupling coefficient $\kappa_0 = N_0 S C_0 \omega_0^2/(2cn_D)$ with $n_D = (1 + \chi_D^{(1)})^{1/2}$ being the refractive index of the background (substrate) material.

APPENDIX C: MULTISCALE EXPANSION AND THE DERIVATION OF THE NONLINEAR ENVELOPE EQUATION

We solve the equations for $q_{\mu\alpha}$ and H_μ ($\mu = d,\ f,\ s,\ t$) by using the method of multiple scales [30,31,42]. Take the asymptotic expansion $q_{f\alpha} = \lambda q_{f\alpha}^{(1)} + \lambda^2 q_{f\alpha}^{(2)} + \lambda^3 q_{f\alpha}^{(3)} + \cdots$, $q_{d\alpha} = \lambda^2 q_{d\alpha}^{(2)} + \lambda^3 q_{d\alpha}^{(3)} + \cdots$, $q_{s\alpha} = \lambda^2 q_{s\alpha}^{(2)} + \lambda^3 q_{s\alpha}^{(3)} + \cdots$, $q_{t\alpha} = \lambda^3 q_{t\alpha}^{(3)} + \cdots$, and $H_f = \lambda H_f^{(1)} + \lambda^2 H_f^{(2)} + \lambda^3 H_f^{(3)} + \cdots$, where λ is a dimensionless small parameter characterizing the amplitude of the incident magnetic field. All quantities on the right-hand side of the expansion are assumed as functions of the multiscale variables $x_1 = \lambda x$, $y_1 = \lambda y$, $z_j = \lambda^j z$ ($j = 0,\ 1,\ 2$), and $t_j = \lambda^j t$ ($j = 0,\ 1$). Substituting this expansion into the Eqs. (B2) and (B3) and comparing the coefficients of λ^j ($j = 1, 2, 3, \ldots$), we obtain a chain of linear but inhomogeneous equations which can be solved order by order.

The first-order ($j = 1$) solution is given by

$$H_f^{(1)} = Fe^{i(kz_0 - \delta t_0)}, \tag{C1a}$$

$$q_{f1}^{(1)} = \frac{-ig\omega_0 D_2(\delta)F}{D_1(\delta)D_2(\delta) - \Omega^4}e^{i(kz_0 - \delta t_0)}, \tag{C1b}$$

$$q_{f2}^{(1)} = \frac{-ig\omega_0 \Omega^2 F}{D_1(\delta)D_2(\delta) - \Omega^4}e^{i(kz_0 - \delta t_0)}, \tag{C1c}$$

where $D_j(l\delta) = \omega_0^2 - l^2(\omega_0 + \delta)^2 - il\gamma_j(\omega_0 + \delta)$ ($j, l = 1, 2$), F is a yet to be determined envelope function, and K is the linear dispersion relation [see Eq. (6) in the main text] given by

$$K = \frac{n_D}{c}\delta + \frac{\kappa_0 g\omega_0 D_2(\delta)}{D_1(\delta)D_2(\delta) - \Omega^4}. \tag{C2}$$

At the second order ($j = 2$), we get the solution

$$q_{f1}^{(2)} = \frac{-ig\omega_0 D_2(\delta)^2[2i(\omega_0 + \delta) - \gamma_1] - ig\omega_0\Omega^4[2i(\omega_0 + \delta) - \gamma_2]}{(D_1(\delta)D_2(\delta) - \Omega^4)^2}\frac{\partial F}{\partial t_1}e^{i(kz_0 - \delta t_0)}, \tag{C3a}$$

$$q_{f2}^{(2)} = \frac{-ig\omega_0 D_1(\delta)\Omega^2[2i(\omega_0 + \delta) - \gamma_2] - ig\omega_0 D_2(\delta)\Omega^2[2i(\omega_0 + \delta) - \gamma_1]}{(D_1(\delta)D_2(\delta) - \Omega^4)^2}\frac{\partial F}{\partial t_1}e^{i(kz_0 - \delta t_0)},$$

$$q_{d1}^{(2)} = -\frac{2g^2\omega_0^2\left(\alpha_1\omega_0^2|D_2(\delta)|^2 + \alpha_2\Omega^6\right)}{\left(\omega_0^4 - \Omega^4\right)|D_1(\delta)D_2(\delta) - \Omega^4|^2}|F|^2 e^{-2\bar{\alpha}z_2}, \tag{C3b}$$

$$q_{d2}^{(2)} = -\frac{2g^2\omega_0^2\left(\alpha_1\Omega^2|D_2(\delta)|^2 + \alpha_2\omega_0^2\Omega^4\right)}{\left(\omega_0^4 - \Omega^4\right)|D_1(\delta)D_2(\delta) - \Omega^4|^2}|F|^2 e^{-2\bar{\alpha}z_2},$$

$$q_{s1}^{(2)} = \frac{g^2\omega_0^2[\alpha_1(D_2(\delta)^2 D_2(2\delta) + \alpha_2\Omega^6]}{[D_1(2\delta)D_2(2\delta) - \Omega^4][D_1(\delta)D_2(\delta) - \Omega^4]^2}F^2 e^{2i(kz_0 - \delta t_0)}, \tag{C3c}$$

$$q_{s2}^{(2)} = \frac{g^2\omega_0^2[\alpha_1(D_2(\delta)^2\Omega^2 + \alpha_2 D_1(2\delta)\Omega^4]}{[D_1(2\delta)D_2(2\delta) - \Omega^4][D_1(\delta)D_2(\delta) - \Omega^4]^2}F^2 e^{2i(kz_0 - \delta t_0)}, \tag{C3d}$$

where $\bar{\alpha} = \lambda^{-2}\alpha_m$ and $\alpha_m \equiv \mathrm{Im}(K)$. A solvability (i.e., divergence-free) condition requires the envelope function F to satisfy the equation

$$i\left(\frac{\partial F}{\partial z_1} + \frac{1}{V_g}\frac{\partial F}{\partial t_1}\right) = 0, \tag{C4}$$

with $V_g = (\partial K/\partial\delta)^{-1}$ being the group velocity of the envelope F.

With the above solutions, we can go to third order. By the solvability condition at this order, we obtain

$$i\frac{\partial F}{\partial z_2} - \frac{1}{2}K_2\frac{\partial^2 F}{\partial t_1^2} + \frac{c}{2\omega_0 n_D}\left(\frac{\partial^2}{\partial x_1^2} + \frac{\partial^2}{\partial y_1^2}\right)F + \frac{\omega_0}{2cn_D}\chi^{(3)}|F|^2 F e^{-2\bar{\alpha}z_2} = 0, \tag{C5}$$

where $K_2 \equiv \partial^2 K/\partial\delta^2$ is dispersion coefficient and $\chi^{(3)}$ is the third-order nonlinear magnetic susceptibility that results from the self-phase modulation, with the explicit expression given by Eq. (10) of the main text. By combining Eqs. (C4) and (C5) and returning to the original variables, we obtain Eq. (9) of the main text.

[1] G. I. Eleftheriad and K. G. Balmain, *Negative-Refraction Metamaterials: Fundamental Principles and Applications* (John Wiley & Sons, New Jersey, 2005).

[2] F. Marqués, R. Martín, and M. Sorolla, *Metamaterials with Negative Parameters: Theory, Design, and Microwave Applications* (John Wiley & Sons, New Jersey, 2008).

[3] W. Cai and V. Shalaev, *Optical Metamaterials: Fundamentals and Applications* (Springer, New York, 2009).

[4] *Metamaterials: Theory, Design, and Applications*, edited by T. J. Cui, D. R. Smith, and R. Liu (Springer, New York, 2010).

[5] Y. Liu and X. Zhang, Metamaterials: A new frontier of science and technology, Chem. Soc. Rev. **40**, 2494 (2011).

[6] *Nonlinear, Tunable and Active Metamaterials*, edited by I. V. Shadrivov, M. Lapine, and Y. S. Kivshar (Springer, Switzerland, 2015).

[7] L. D. Landau, E. M. Liftshitz, and L. P. Pitaevskii, *Electrodynamics of Continuous Media* (Pergamon, New York, 1984).

[8] J. B. Pendry, A. J. Holden, D. J. Robbins, and W. J. Stewart, Magnetism from conductors and enhanced nonlinear phenomena, IEEE Trans. Microwave Theory Tech. **47**, 2075 (1999).

[9] E. Nahvi, I. Liberal, and N. Engheta, Nonperturbative effective magnetic nonlinearity in ENZ media doped with Kerr dielectric inclusions, ACS Photon. **6**, 2823 (2019).

[10] M. Lapine, I. V. Shadrivov, and Y. S. Kivshar, Colloquium: Nonlinear metamaterials, Rev. Mod. Phys. **86**, 1093 (2014).

[11] N. M. Litchinitser, Nonlinear optics in metamaterials, Adv. Phys.: X **3**, 1367628 (2018).

[12] A. Krasnok, M. Tymchenko, and A. Alú, Nonlinear metasurfaces: A paradigm shift in nonlinear optics, Mater. Today (Oxford, U. K.) **21**, 8 (2018).

[13] B. Wang, J. Zhou, T. Koschny, and C. M. Soukoulis, Nonlinear properties of split-ring resonators, Opt. Express **16**, 16058 (2008).

[14] I. V. Shadrivov, A. B. Kozyrev, D. W. van der Weide, and Y. S. Kivshar, Nonlinear magnetic metamaterials, Opt. Express **16**, 20266 (2008).

[15] E. Poutrina, D. Huang, and D. R. Smith, Analysis of nonlinear electromagnetic metamaterials, New J. Phys. **12**, 093010 (2010), and references therein.

[16] E. Poutrina, D. Huang, Y. Urzhumov, and D. R. Smith, Nonlinear oscillator metamaterial model: Numerical and experimental verification, Opt. Express **19**, 8312 (2011).

[17] D. Huang, E. Poutrina, and D. R. Smith, Analysis of the power dependent tuning of a varactor-loaded metamaterial at microwave frequencies, Appl. Phys. Lett. **96**, 104104 (2010).

[18] S. Larouche, A. Rose, E. Poutrina, D. Huang, and D. R. Smith, Experimental determination of the quadratic nonlinear magnetic susceptibility of a varactor-loaded split ring resonator metamaterial, Appl. Phys. Lett. **97**, 011109 (2010).

[19] M. A. Lopez, M. J. Freire, J. M. Algarin, V. C. Behr, P. M. Jakob, and R. Marqués, Nonlinear split-ring metamaterial slabs for magnetic resonance imaging, Appl. Phys. Lett. **98**, 133508 (2011).

[20] D. Huang, A. Rose, E. Poutrina, S. Larouche, and D. R. Smith, Wave mixing in nonlinear magnetic metacrystal, Appl. Phys. Lett. **98**, 204102 (2011).

[21] D. Huang, E. Poutrina, H. Zheng, and D. R. Smith, Design and experimental characterization of nonlinear metamaterials, J. Opt. Soc. Am. B **28**, 2925 (2011).

[22] S. Zhang, D. A. Genov, Y. Wang, M. Liu, and X. Zhang, Plasmon-Induced Transparency in Metamaterials, Phys. Rev. Lett. **101**, 047401 (2008).

[23] N. Papasimakis, V. A. Fedotov, and N. I. Zheludev, Metamaterial Analog of Electromagnetically Induced Transparency, Phys. Rev. Lett. **101**, 253903 (2006).

[24] P. Tassin, L. Zhang, T. Koschny, E. N. Economou, and C. M. Soukoulis, Low-Loss Metamaterials Based on Classical Electromagnetically Induced Transparency, Phys. Rev. Lett. **102**, 053901 (2009).

[25] R. Singh, C. Rockstuhl, F. Lederer, and W. Zhang, Coupling between a dark and a bright eigenmode in a terahertz metamaterial, Phys. Rev. B **79**, 085111 (2009).

[26] N. Liu, L. Langguth, T. Weiss, J. Kästel, M. Fleischhauer, T. Pfau, and H. Giessen, Plasmonic analog of electromagnetically induced transparency at the Drude damping limit, Nat. Mater. **8**, 758 (2009).

[27] N. Liu, T. Weiss, M. Mesch, L. Langguth, U. Eigenthaler, M. Hirscher, C. Sönnichsen, and H. Giessen, Planar metamaterial analogue of electromagnetically induced transparency for plasmonic sensing, Nano Lett. **10**, 1103 (2010).

[28] N. Liu, M. Hentschel, T. Weiss, A. P. Alivisatos, and H. Giessen, Three-dimensional plasmon rulers, Science **332**, 1407 (2011).

[29] J. Gu, R. Singh, X. Liu, X. Zhang, Y. Ma, S. Zhang, S. A. Maier, Z. Tian, A. K. Azad, H.-T. Chen, A. J. Taylor, J. Han, and W. Zhang, Active control of electromagnetically induced transparency analog in terahertz metamaterials, Nat. Commun. **3**, 1151 (2012).

[30] Z. Bai and G. Huang, Plasmon dromions in a metamaterial via plasmon-induced transparency, Phys. Rev. A **93**, 013818 (2016).

[31] Q. Zhang, Z. Bai, and G. Huang, Analogue of double-Λ-type atomic medium and vector plasmonic dromions in a metamaterial, Opt. Express **25**, 25447 (2017).

[32] M. Fleischhauer, A. Imamoglu, and J. P. Marangos, Electromagnetically induced transparency: Optics in coherent media, Rev. Mod. Phys. **77**, 633 (2005).

[33] P. W. Milonni, *Fast Light, Slow Light and Left-Handed Light* (IOP Publishing, London, 2005).

[34] J. B. Khurgin, Slow light in various media: A tutorial, Adv. Opt. Photon. **2**, 287 (2010).

[35] I. Novikova, R. L. Walsworth, and Y. Xiao, Electromagnetically induced transparency-based slow and stored light in warm atoms, Laser Photon. Rev. **6**, 333 (2012).

[36] Y. Chen, Z. Bai, and G. Huang, Ultraslow optical solitons and their storage and retrieval in an ultracold ladder-type atomic system, Phys. Rev. A **89**, 023835 (2014).

[37] Such simplified treatment is for facilitating the numerical simulation without significantly changing the result of the simulation.

[38] Z. Bai, G. Huang, L. Liu, and S. Zhang, Giant Kerr nonlinearity and low-power gigahertz solitons via plasmon-induced transparency, Sci. Rep. **5**, 13780 (2015).

[39] Z. Bai, D. Xu, and G. Huang, Storage and retrieval of electromagnetic waves with orbital angular momentum via plasmon-induced transparency, Opt. Express **25**, 785 (2017).

[40] Z. Bai, Q. Zhang, and G. Huang, Nonlinear polaritons in metamaterials with plasmon-induced transparency [Invited], Chin. Opt. Lett. **17**, 012501 (2019).

[41] M. R. Shcherbakov, D. N. Neshev, B. Hopkins, A. S. Shorokhov, I. Staude, E. V. Melik-Gaykazyan, M. Decker, A. A. Ezhov, A. E. Miroshnichenko, I. Brener, A. A. Fedyanin, and Y. S. Kivshar, Enhanced third-harmonic generation in silicon nanoparticles driven by magnetic response, Nano Lett. **14**, 6488 (2014).

[42] A. C. Newell and J. V. Moloney, *Nonlinear Optics* (Addison-Wesley, California, 1992).

[43] N. Lazarides, M. Eleftheriou, and G. P. Tsironis, Discrete Breathers in Nonlinear Magnetic Metamaterials, Phys. Rev. Lett. **97**, 157406 (2006).

[44] N. Lazarides, G. P. Tsironis, and Y. S. Kivshar, Surface breathers in discrete magnetic metamaterials, Phys. Rev. E **77**, 065601 (2008).

[45] W. Cui, Y. Zhu, H. Li, and S. Liu, Self-induced gap solitons in nonlinear magnetic metamaterials, Phys. Rev. E **80**, 036608 (2009).